Energy Equip. Sys. / Vol. 8/No. 4/Dec. 2020/ 367-388

ENERGY EQUIPSYS

Energy Equipment and Systems

http://energyequipsys.ut.ac.ir
www.energyequipsys.com

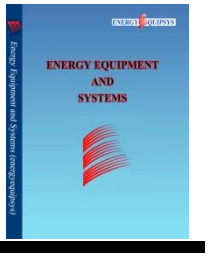

Film cooling simulation on an entire gas turbine blade with square pulsed coolant injection

Authors

Seyyed Mehdi Hosseini Baghdad Abadi [a]
Saadat Zirak [a*]
Mehran Rajabi Zargarabadi[a]

[a] Faculty of Mechanical Engineering, Semnan University, Semnan, Iran

Article history:

Received : 10 December 2019
Accepted : 17 May 2020

ABSTRACT

Film cooling is an effective method to keep the gas turbine blades from high temperature gases and thermal stresses. Square pulsating film cooling on different sections of a modified NASA C3X blade is numerically investigated. Temperature distribution and film cooling performance are investigated for various blowing ratios of 0.5, 0.75, 1.0, 1.5, 2 and 2.5 in pulse frequency of 50Hz. Reynolds-Averaged Navier-Stokes equations for steady and pulsating injection considered. The shear stress transport (SST $k-\omega$) model applied for turbulence effects. Simulations are performed using finite volume method. Obtained results show different findings of pulsating film cooling on the various blade surfaces. For large blowing ratios, averaged pulsed film covering effectiveness at leading edge and pressure side of blade is reduced compared to small and middle values of blowing ratios. This trend is reversed in the suction side. Reynolds number of mainstream has the maximum effect on film effectiveness distribution on pressure section. The averaged centerline pulsed film coolant performance on the pressure surface and leading edge at blowing ratio of 0.5 and for suction side at blowing ratio 2.5 was maximum.

Keywords: Numerical Simulation; Blade; Film Cooling; Square Pulsation; Effectiveness.

1. Introduction

At the specified inlet temperature, the compressor and turbine are characterized by known efficiency and pressure ratio [1]. Higher turbine entrance temperature is now required to obtain more cycle efficiencies in new gas turbines. The inlet temperature enhancement can reason for failure of turbine blades. Desirable lifetime of turbine vanes can be attained with an effective surface cooling method such as film cooling [2]. Various cooling systems are applied to maintain turbine blades from mainstream hot air. These systems can be classified as surface film covering and internal cooling [3]. Film cooling is one of the best and the most advanced cooling ways broadly applied in today's gas turbine to cool components subjected to high temperatures such as vanes and blades [2]. For steady state conditions, film cooling efficiency has been studied for different flow parameters. Mousavi and Rahnama numerically presented optimal shape on a flat wall with film cooling and impingement systems. Results showed that

* Corresponding author: Saadat Zirak
[a] Faculty of Mechanical Engineering, Semnan University, Semnan, Iran
Email: s_zirak@semnan.ac.ir

for optimum design, 44% less cooling air consumption obtained with usage both optimized cooling methods [3]. Park et al. [4] considered the influence of shape parameters on film coolant covering performance. Results showed that film cooling effectiveness enhanced with increasing the forward and side developed angle and the measurement length was less. With incrementing the density ratio, the film cooling effectiveness improved but the influence of blowing ratio was not stable.

Abdelmohimen and Mohiuddin [5] added secondary holes to injection holes with compound angle to reinforce turbine operation by increasing film cooling effectiveness. Study for different blowing ratios carried out. The obtained results showed that added holes help maintain the base injection jet to downstream the test plate and leading to higher film covering particularly for large blowing ratios. Chen et al. [6] numerically investigated the influence of internal channel flow on the film cooling effectiveness. With changing the blowing ratios and lateral flow velocity, adiabatic film cooling effectiveness changed. Internal crossflow had a significant impact on the film cooling effectiveness. Increased coolant cover obtained at internal crossflow situations. For this case, vortexes inside the hole had not the samee direction with counter rotating vortex pairs at the downstream.

Qingzong et al. [7] studied the film cooling efficiency at the downstream injection holes with considering the endwall step. $SST\ k-\omega$ model was applied to perform the calculations of turbulence effects. By raising the blowing ratio from 0.6 to 1.2, the adiabatic film cooling effectiveness reduced at upstream and downstream of the coolant injection holes because of lift-off promotion. The findings showed that the coolant covering effect severely depends on the axial location of the injection hole. Locating the injection holes at downstream of leading edge showed a slight effect on the film cooling and consequently, relatively uniform cooling covering on the surface. Mousavi et al. [8] applied several methods for maximization the film cooling of turbine blade. A novel optimal procedure was presented for cooling the blade surfaces that it improved the overall turbine efficiency and output power by 17% and 4.68%, respectively.

Zhang et al. [9] measured the influences of height and placing of the vortices producer on flow structure and heat transfer specifications of the film cooling on the flat surface. They found out that as the height of the vortex generator increments the film cooling effectiveness that first it had an increasing trend and then a decreasing one. In addition, the optimum increase in film cooling performance improved with increasing blowing ratio from 0.5 to 1.5. That is infeasible to ignore the oscillation generated by variable alternative interaction between stator and rotor or by pulsating mainflow. Square wave oscillation flow is used in studies because pressure oscillations in the mainstream can result from film cooling in complete opening or closer condition.

Liu and Luo [10] studied pulsating film covering on fluid pattern and heat transfer specifications of a turbine. They used the 3D unsteady Averaged Reynolds Navier-Stokes equations. To consider Turbulent effects, the SST $k-\omega$ model used. Thermal and aerodynamic characteristics and film coverage of the blade wall are studied numerically. The effect of coolant air causes that at a moment, temperature distribution on the blade surfaces is non-uniform. The gas temperature near the pressure surface is higher than gas temperature near the suction section. Hosseini Baghdad Abadi et al. [11] investigated the film cooling coverage with sinusoidal wave pulsating injection on the flat plate at various frequencies. The obtained results showed that with increasing frequency, the flow-off and flow-on interruption decreased and consequently, the instantaneous effectiveness variations was slower than that for the low frequencies. Womack et al. [12] studied film cooling injection holes with pulsation exposed to oscillating wakes. At low frequencies, wake timing had a considerable influence on the instantaneous film cooling effectiveness, however generally wake had very slight effect on the averaged film cooling performance. Borup et al. [13] determined the effects of unsteady oscillating mainstream eventuating

from the interaction between blades and vanes of turbine on the film cooling effectiveness. The pulsating unsteadiness was specified by alternative cycles of slow mainstream that allowed the cooling air to diffuse into the mainstream along the centerline.

Due to difference in performance of film cooling in blade and flat plate, as well as need to examine the effect of pulsation on it, in this research the influence of oscillating cooled gas flow on film cooling effectiveness of different surfaces of modified NASA C3X blade are studied and discussed.

2. Geometry, governing equations and computational model

Geometry of problem involves NASA C3X blade which includes three rows of injection holes, one row at leading edge and the other two rows on suction and pressure sides of the blade as demonstrated in Fig. 1 The injection holes diameter is 2mm. The ratio of hole length (depth) to diameter for leading edge, suction and pressure surfaces were 5.5, 6.5 and 6.1, respectively. Injection angle is 90° for leading edge and 25° for pressure and suction surfaces. Three plenums are considered for cooling air at each section as shown in Fig.1.

Figure 2 shows 3D computational region, dimensions and boundary conditions.

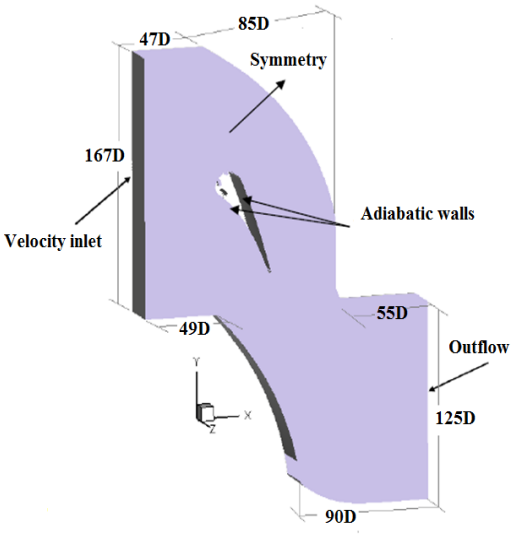

Fig. 2. Geometry, computational region, and blade boundary conditions

Mesh quality is an important factor for calculating fluid flow. Therefore, it has been attempted to create the appropriate mesh in the mentioned domain [14]. Structural hexahedron cells are used to mesh the geometry.

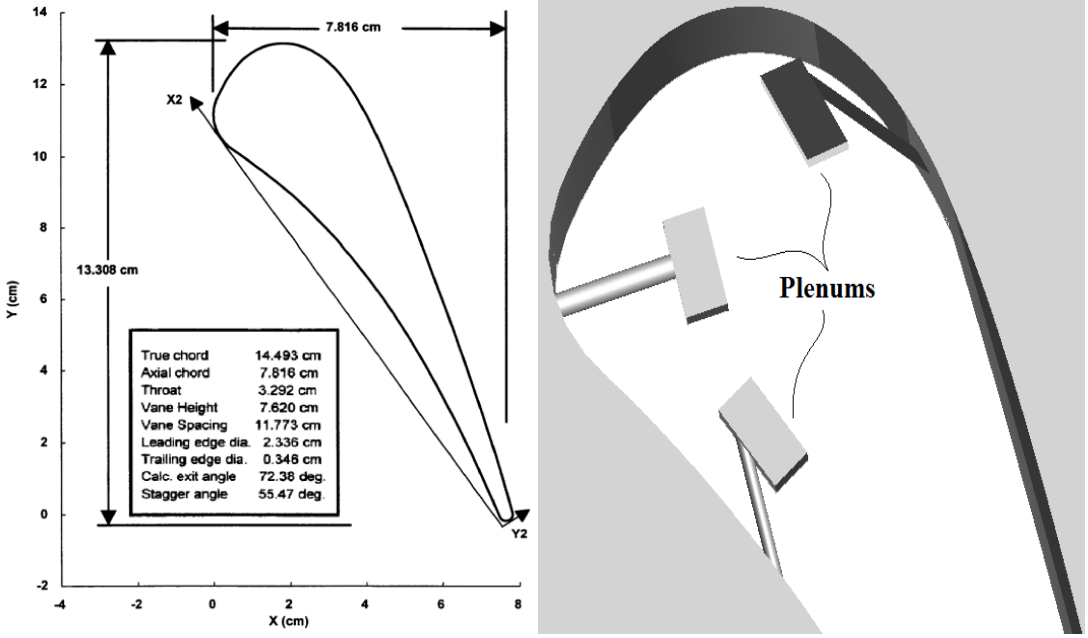

Fig. 1. Blade Geometry and plenums of cooling air injection

Figure 3 shows the mesh geometry of the turbine blade surface and the regions near the injection holes.

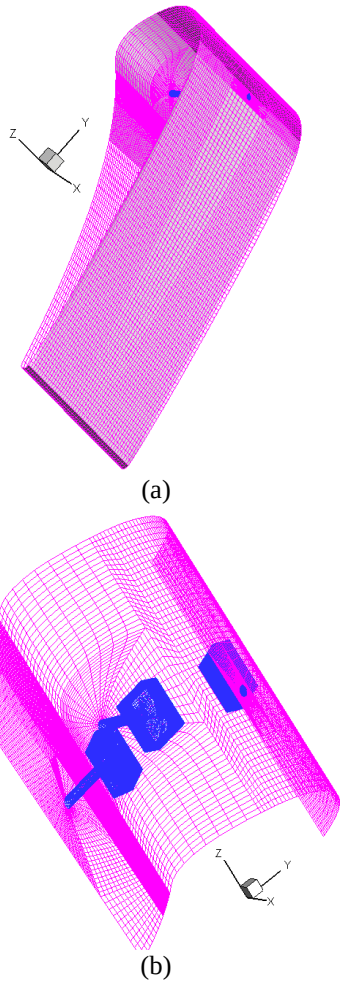

Fig. 3. Computational mesh of (a) blade wall and (b) regions around the injection holes

To check grid independency, three different grids with 2502500, 4345700 and 6654900 computational cells was considered. Centerline adiabatic temperature at steady state for three grids is shown in Fig. 4. As can be seen, the differences for the two last grids are less than 2% at all distances, and as a result the mesh with 4345700 cells was used for further analysis.

The mass, momentum, energy governing equations are given as follows:

$$\frac{\partial}{\partial x_i}(\rho u_i) = 0 \tag{1}$$

$$\frac{\partial(\rho u_i)}{\partial t} + \frac{\partial}{\partial x_i}(\rho u_i u_j) = \rho\overrightarrow{g_j} - \frac{\partial P}{\partial x_j} + \frac{\partial}{\partial x_i}(\tau_{ij} - \rho\overline{\acute{u}_i\acute{u}_j}) + F_j \tag{2}$$

$$\frac{\partial}{\partial x_i}(\rho c_p u_i T) = \frac{\partial}{\partial x_i}\left(k\frac{\partial T}{\partial x_i} - \rho c_p\,\overline{\acute{u}_i\acute{T}}\right) + \mu\phi + S_h \tag{3}$$

where τ_{ij} is the symmetric stress tensor described as:

$$\tau_{ij} = \mu\left(\frac{\partial u_i}{\partial x_j} + \frac{\partial u_j}{\partial x_i} - \frac{2}{3}\,\delta_{ij}\frac{\partial u_k}{\partial x_k}\right) \tag{4}$$

$\mu\phi$ is the viscous dissipation and k is the thermal conductivity.

Film cooling effectiveness, η, is expressed as:

$$\eta = \frac{T_\infty - T_{aw}}{T_\infty - T_{coolant\ air}} \tag{5}$$

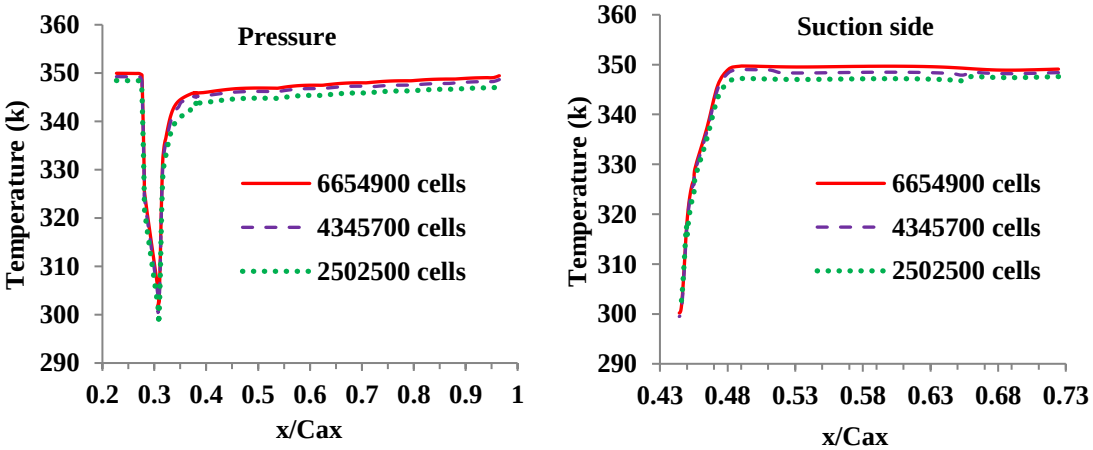

Fig. 4. Surface temperature contours on suction side and pressure surface for three different grids

where, T_∞ is mainstream air temperature, T_{aw} is adiabatic wall temperature which is obtained from simulation or measurement, and $T_{coolant\ air}$ is injection coolant air temperature.
Square pulsed wave is defined as:

$$u_{coolant\ air} = \{_{0}^{u} \quad {}^{t<t_a}_{t_a<t<t_b} \quad p = t_b \qquad (6)$$

Because the flow is oscillating and therefore unsteady, that is essential to check time period independent for numerical results. For a square pulsation, the cycles are continued until the analysis results remain the same for successive cycles. Differences of distribution of blade surface effectiveness for 8th and 9th cycles were less than 0.005%; and for 9th and 10th cycles, difference was zero.

For mainstream, flow velocity was considered $20\mathrm{m/s}$ and coolant air flow varied by blowing ratios of 0.5, 0.75, 1, 1.5, 2, and 2.5 ($M = \frac{(\rho u)_{coolant\ air}}{(\rho u)_{main\ stream}}$). Mainstream temperature was 350.15 K and coolant temperature was 300.15 K. Density ratio was 1.166. Turbulence intensity considered 5% for both mainstream and cooling air.

The $SST\ k-\omega$ model has been extensively applied to successfully predict the flow structure and thermal properties of film cooling; the numerical investigations of Mousavi and Rahnama [8], Hosseini Baghdad Abadi et al. [11,15, 26-29], Montomoli et al. [16], Lin and Shih [17], He et al. [18], Ke and Wang [19], Wang et al. [20]. The model incorporates the $k-\omega$ turbulent model and $k-\varepsilon$ model so that the $k-\omega$ is applied in the inner area of the boundary layer and substitutes to the $k-\varepsilon$ in the free shear flow. Menter fully explained and provided details of the $SST\ k-\omega$ model [21]. Boundary conditions of square pulsed velocity profile define with UDF coding at fluent software.
Models and parameters values used in numerical solution are presented at Table 1.

3. Results and Analyses

Model validation determines the degree to which an accurate and valid demonstration model of the actual system [22].
Figure 5 demonstrates wall temperature and pressure around the blade in comparison with Hylton et al. experiment data and numerical results of Zhaoqing and Wang [24] for non-pulsating injection. The most difference between present average pressure around the blade surface with experimental data is 13.8% and with referenced numerical results is 8.4%. Also, most difference in wall temperature at present numerical solution with experiment and other numerical work is 3.7% and 3.2%, respectively. The little differences in the results back to test equipment and the simulation geometry [25].

Table 1 Models and numerical solution parameters

Parameters	Models and parameters
Dimension	*3D*
Solver	Pressure Based
Formulation	Implicit
Pressure-Velocity Coupling algorithm	Simple C
Turbulent model	$SST\ k-\omega$
Pressure discretization	Standard, Second Order
Momentum, turbulence and energy discretization	Second Order Upwind
Time	Unsteady
Number of time step for a Period	20 Time Step
Blowing Ratio	0.5, 0.75, 1, 1.5, 2, 2.5
Frequency	50 Hz

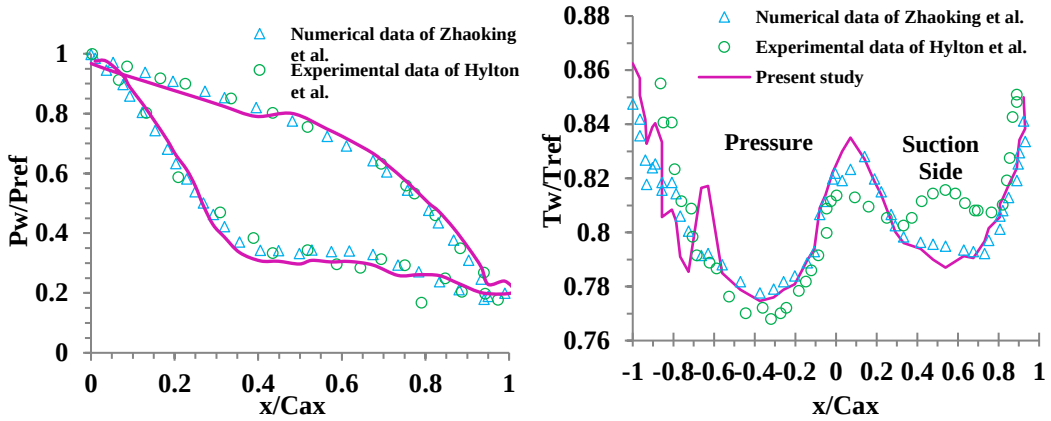

Fig. 5. Calculated pressure and temperature distribution on blade surfaces in comparison with references

3.1. Steady state flow

In Fig. 6, contours of blade temperature distribution are shown for steady state at various blowing ratios. The axises in the figure are in meters. As can be seen, with increasing the blowing ratio from 0.5 to 2.5, due to separation of film cooling on different blade surfaces, blade surface temperature increases at leading edge, pressure and suction surfaces, and in turn, by increasing the blowing ratio the mainstream temperature is reduced due to more penetration of coolant flow into it. Covering coolant film on pressure side is higher than leading edge and the suction side. At leading edge, near the stagnation point, freestream velocity is approximately zero and hence, film cooling formation at this section is difficult [24].

For blowing ratio of 0.5, surface temperature at downstream of injection hole for leading edge and pressure side is less than that for other blowing ratios, and as a result, averaged film cooling effectiveness is larger. For suction side at blowing ratio of 1.5, coolant air covers a wider region of downstream of injection hole than other blowing ratios, and hence, averaged effectiveness for this region is larger. For high blowing ratios, averaged film cooling effectiveness at various blade surfaces is reduced compared to low and medium blowing ratios.

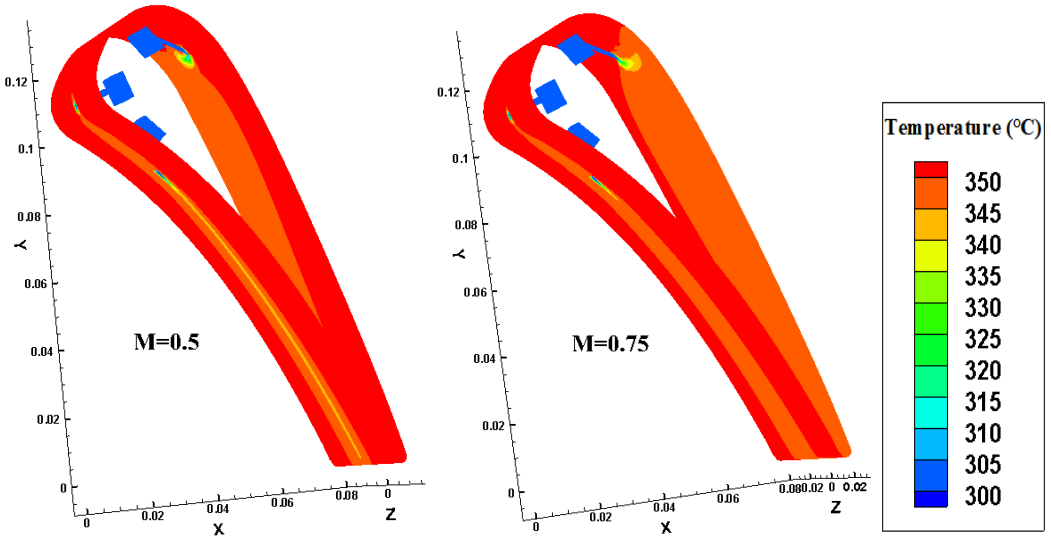

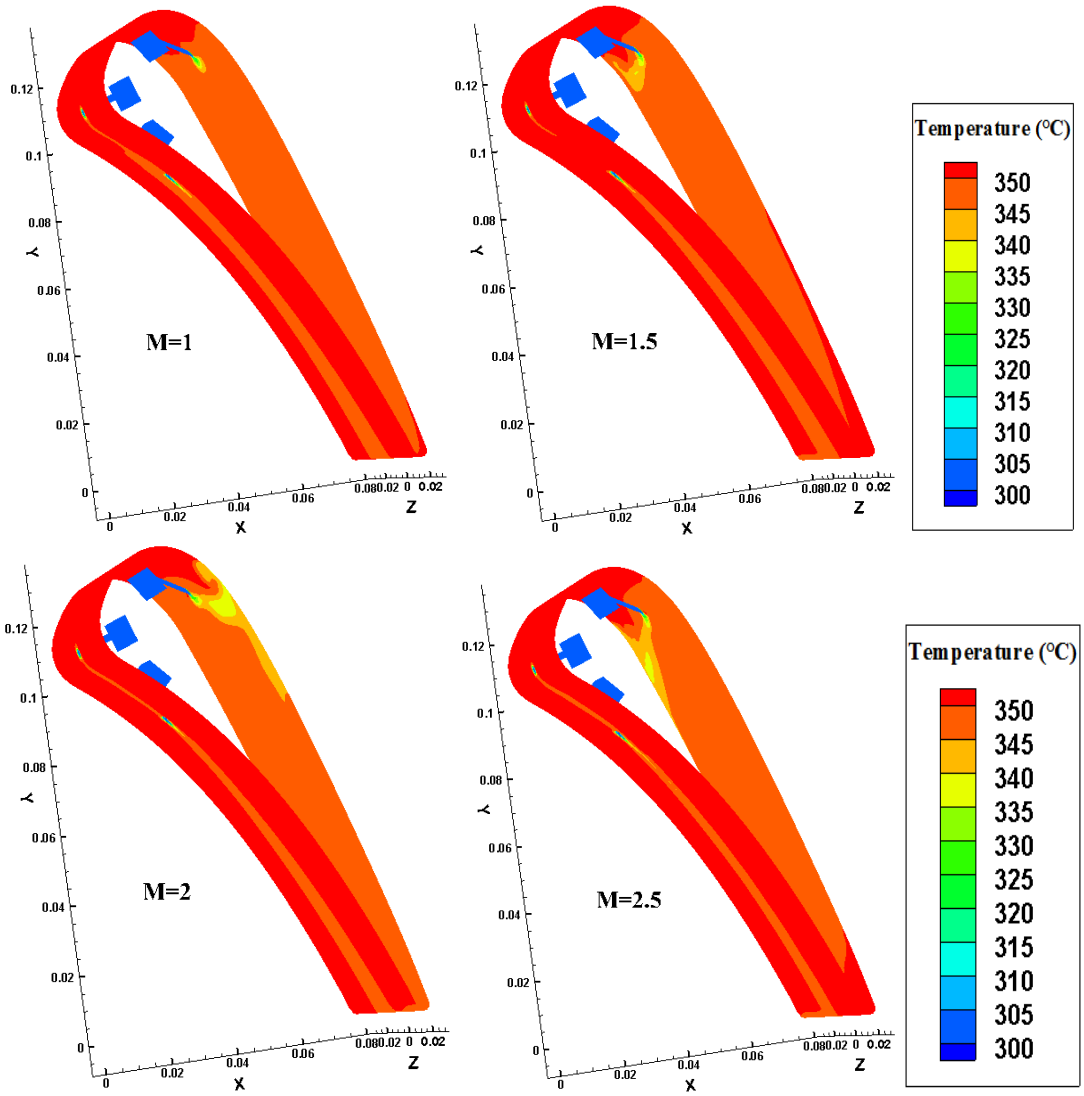

Fig. 6 . Distribution of surface temperature of blade at various blowing ratios

Figure 7 shows velocity contour and streamlines of mainstream and cooling air on blade surface for two blowing ratios of 0.5 and 2. For blowing ratio of 0.5, in comparison with blowing ratio of 2, streamlines of injection air is adhered to leading edge and pressure surfaces, and therefore, film cooling effectiveness is larger. For suction side, a secondary flow is formed at the downstream of injection hole that its base core at blowing ratio of 2 is closer to the injection hole in comparison with blowing ratio of 0.5, causing greater mixing of mainstream and cooling air. For this reason, film cooling effectiveness for suction surface at blowing ratio of 2 is also less than that with blowing ratio of 0.5.

3.2. Square pulsed flow

For square wave flow, temperature contours of blade surfaces at various times of a period for a complete cycle at blowing ratio of 0.5 is shown in Fig. 8. As can be seen, temperature distribution is changed at various time steps at downstream of the injection hole of leading edge, suction and pressure surfaces. Because of curvature the pressure side geometry, cooling air is lifted-off at downstream of injection hole and pushed to more down distances of surface by mainstream. Concave shape of pressure side reinforces this effect. Figure 8 also shows that although the injection flow is on at the beginning of the cycle ($t = 0$) but still does not have sufficient time to form a cooling film on the surface and therefore the wall temperature of blade surfaces is high.

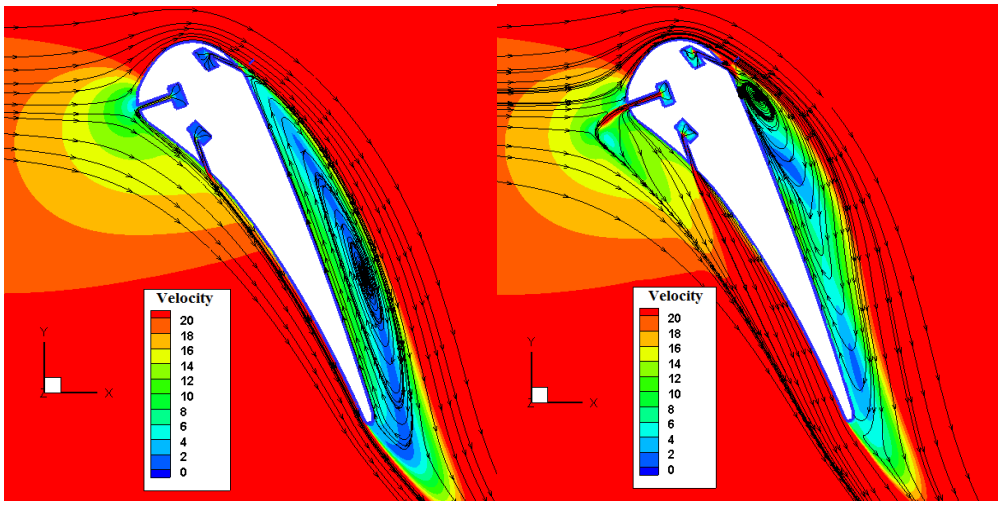

(a) (b)

Fig. 7. Mainstream and cooling air streamlines around the blade surface at blowing ratios of (a) 0.5 (b) 2

Following that, the surface is cooled and with formation of the film cooling, wall temperature of downstream of the injection holes at first half cycle in which the injection flow is on, reaches to its lowest value. By flow-off at second half of a cycle, surface temperature begins to increase and this process is repeated in subsequent cycles.

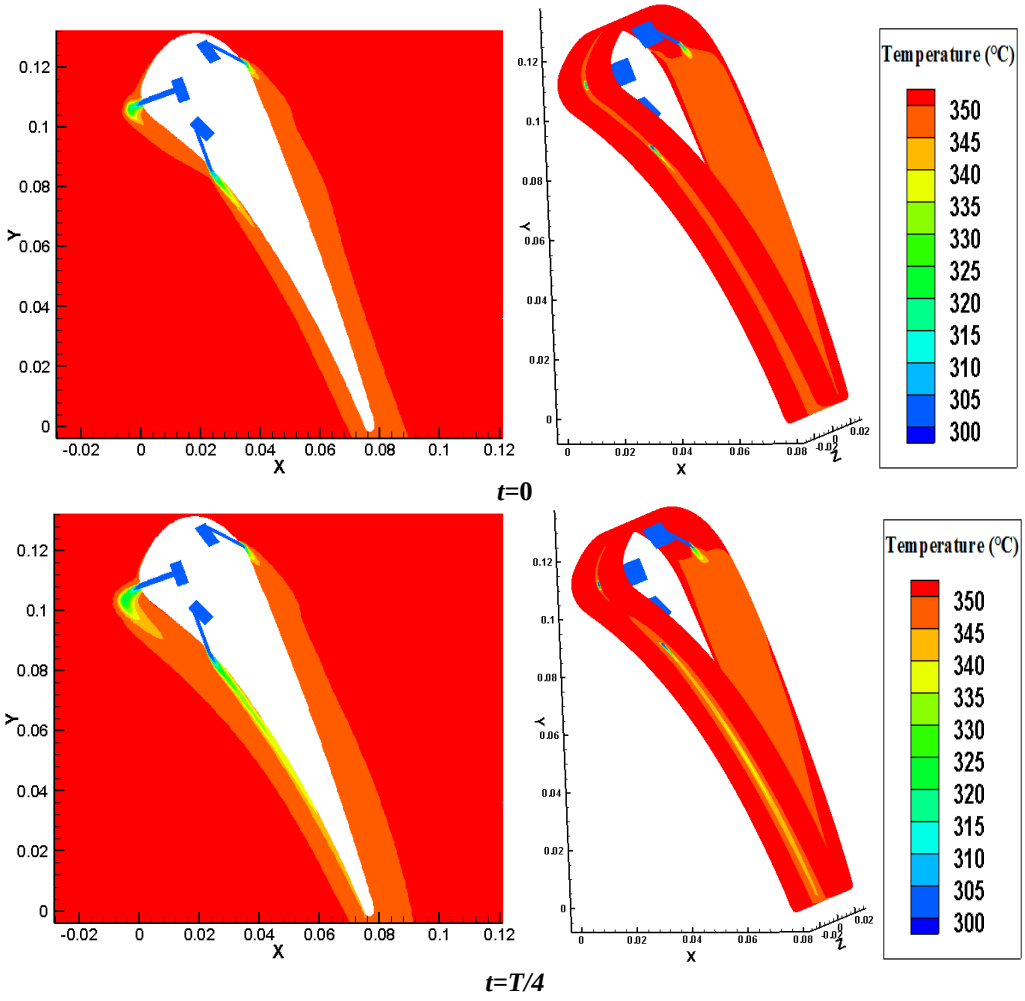

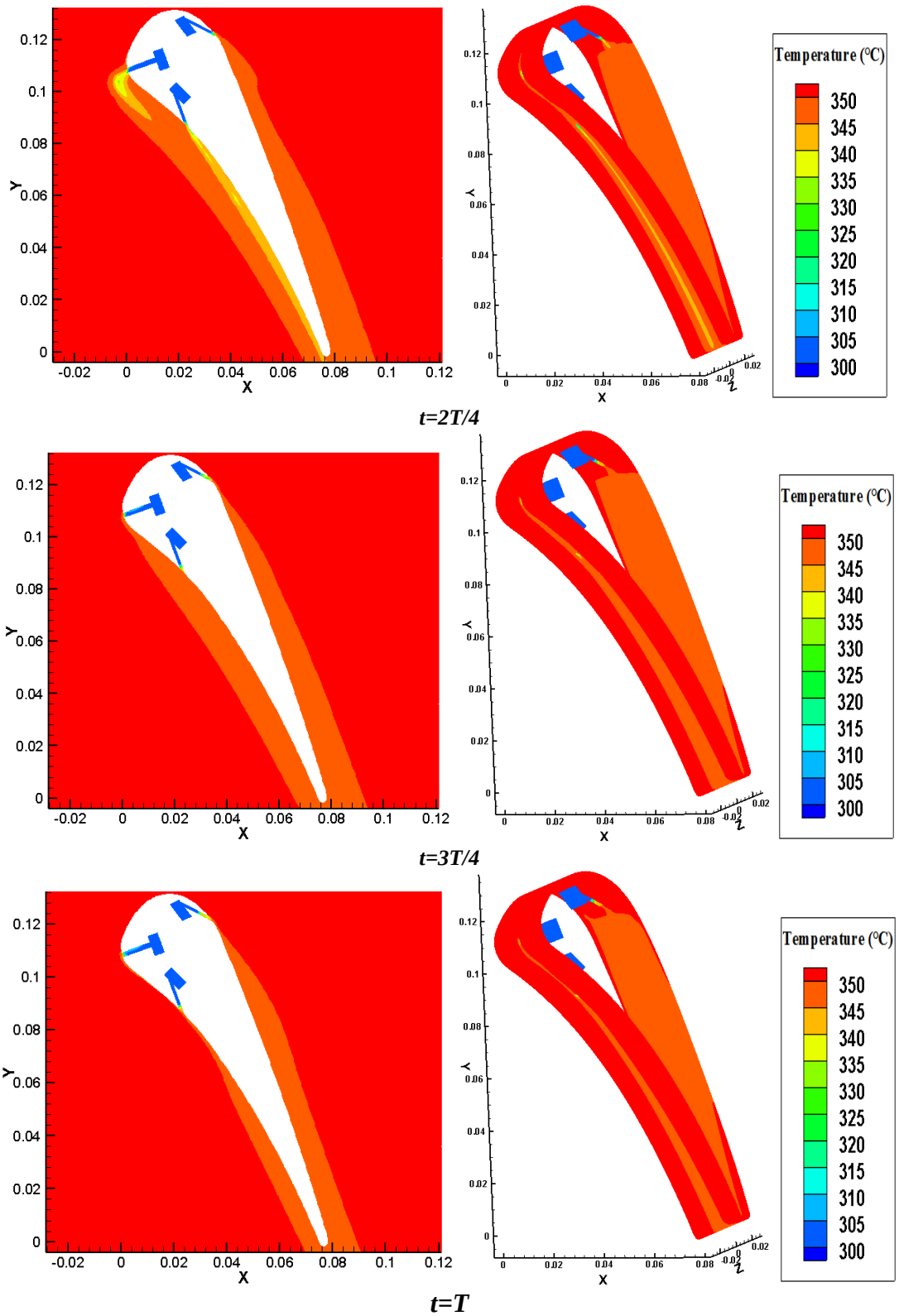

Fig. 8. Temperature distribution of different blade surfaces and its regions around at various time steps of a period with sinusoidal pulsed flow at frequency of 50 Hz and M=0.5

Figure 9 displays effectiveness distribution on blade surface at blowing ratio of 0.5. Effectiveness distribution variations are related to changes of mass flow rate of cooling air at a cycle. Change of coolant mass flow rate at a cycle causes change of size of counter-rotating vortex pair, resulting in a change at surface temperature distribution at any time step. As shown in Fig. 9, at first half of cycle that flow is on and coolant injects on the surface, size of counter-rotating vortex pair increases, and as result, more cooling air is entered to mainstream. In the followings with flow-off the coolant mass flow rate at second half of the cycle, vortex pair also decreases to its smallest size and strength. It should be noted that due to sudden changes in coolant mass flow rate for square pulsed wave (on-off flow at a cycle), size and strength of counter-rotating vortex pairs is rapidly changed and hence affects the wall temperature distribution and, therefore, distribution of film cooling effectiveness at leading edge, suction and pressure surfaces.

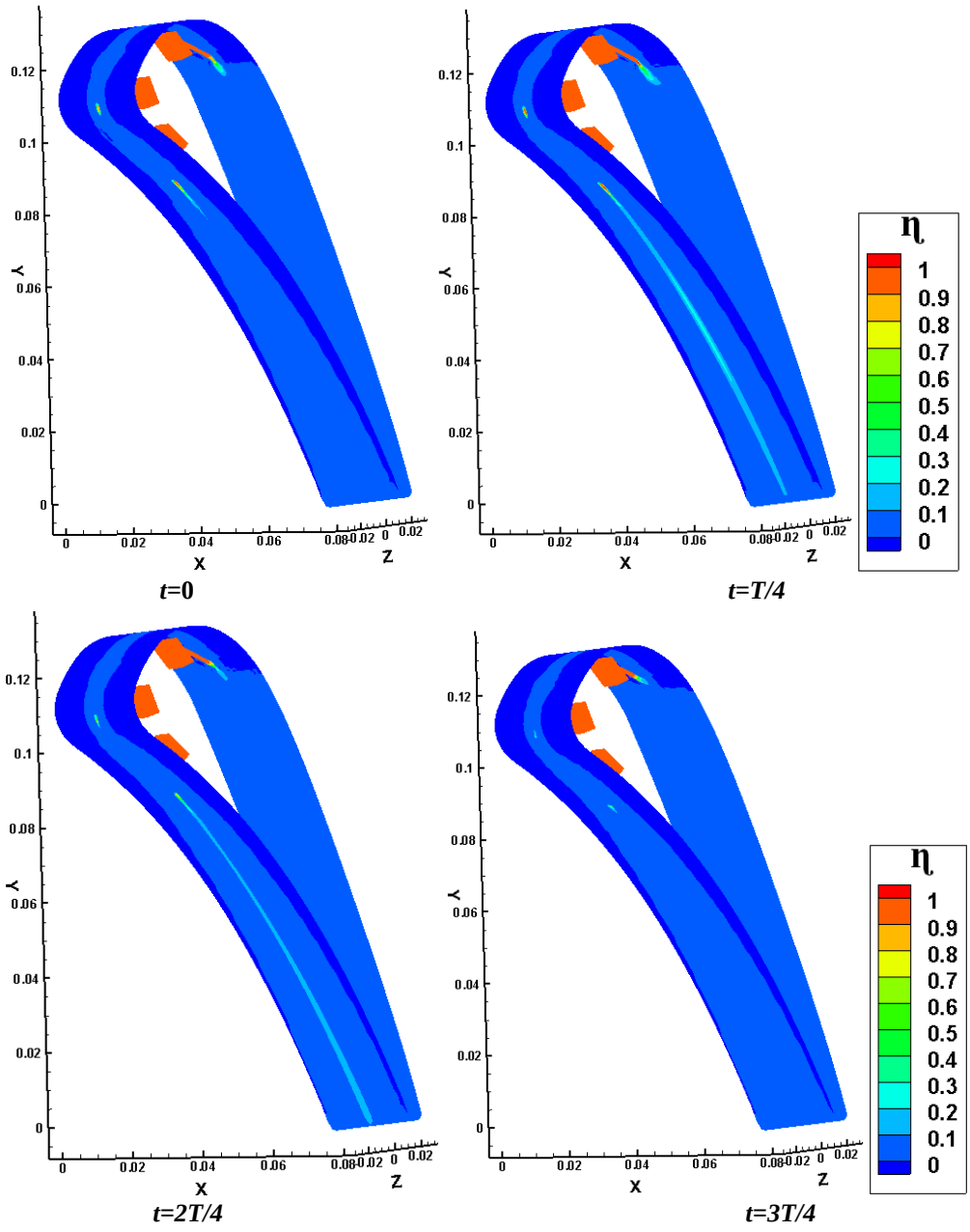

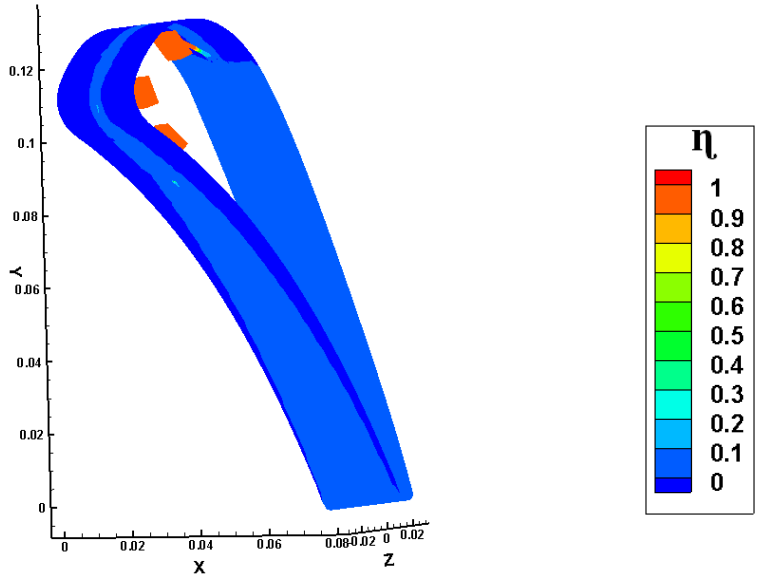

Fig. 9. Contour of blade film cooling effectiveness for various time steps of a cycle of sinusoidal pulsation at frequency of 50 Hz and M=0.5

For square wave flow, contours the surface temperature of blade at various steps in a period time at blowing ratio of 1 is shown in Fig. 10. By increasing the blowing ratio to 1, more cooling air flows into the mainstream, and therefore wider region of mainstream is affected to coolant air compared to blowing ratio of 0.5. By increasing blowing ratio and separation of coolant from the surface after the injection hole of pressure side, coolant air reattach to the surface again at more downstream of the hole and cools the surface. As it is clear from Fig. 10, for sections of leading edge and suction side, separation of cooling air at downstream regions of injection hole is not reattached to the surface and injection air is entered into the mainstream and mixed with it.

By flow-off at the second half of cycle, the coolant air film at leading edge rapidly dissipates and the surface temperature of this section rises rapidly. But for suction and pressure surfaces, even at the end of a cycle, cooling air effect exist on the surface and of course mainstream.

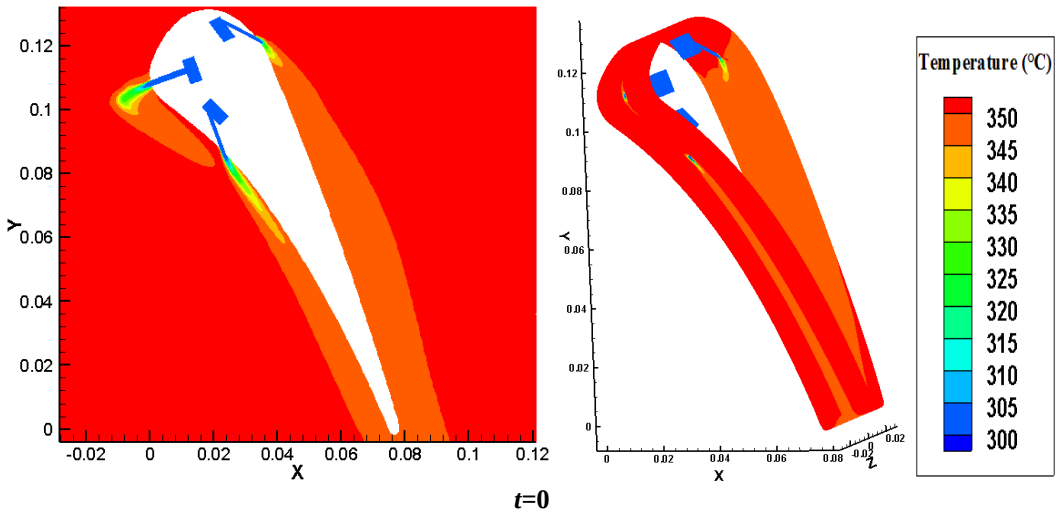

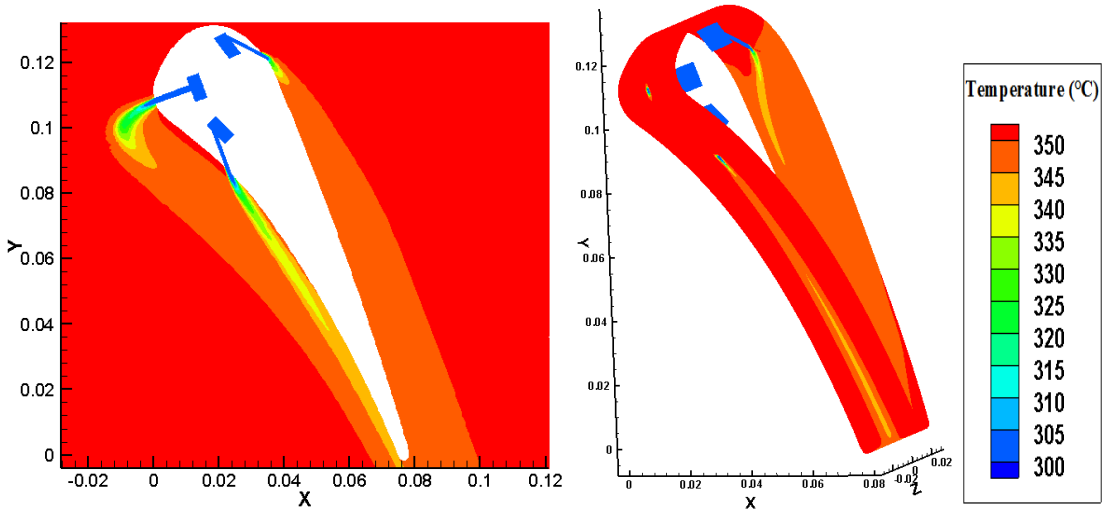

t=T/4

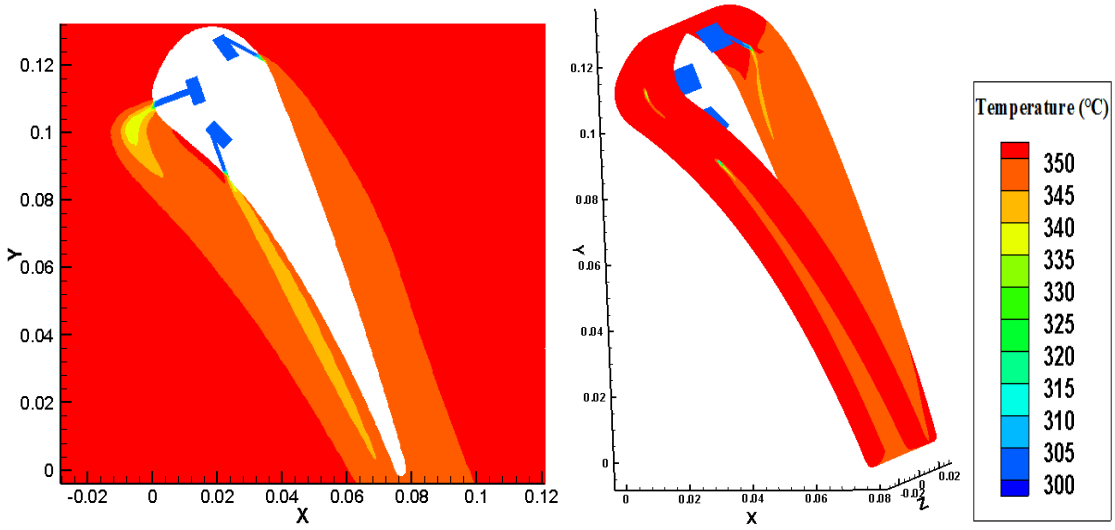

t=2T/4

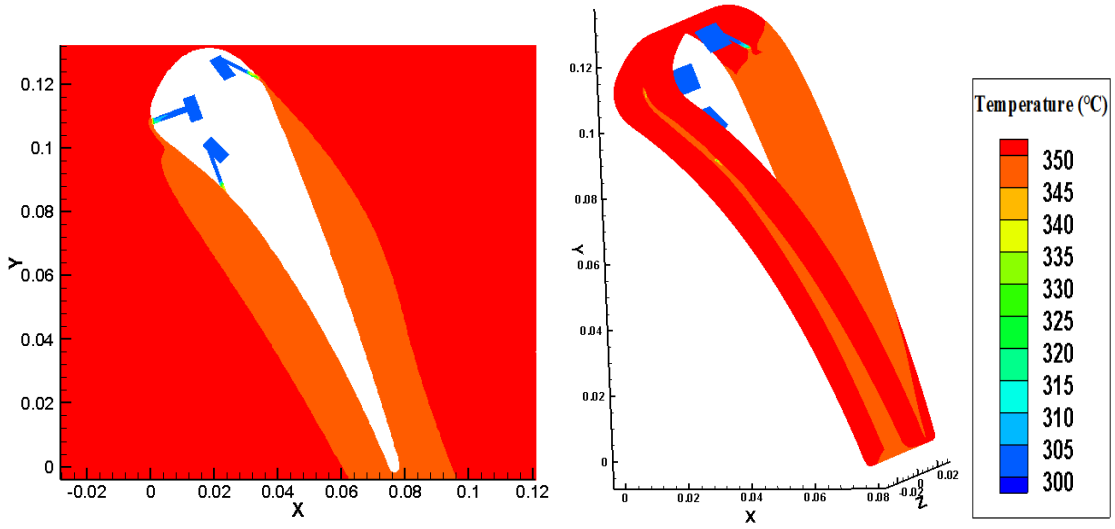

t=3T/4

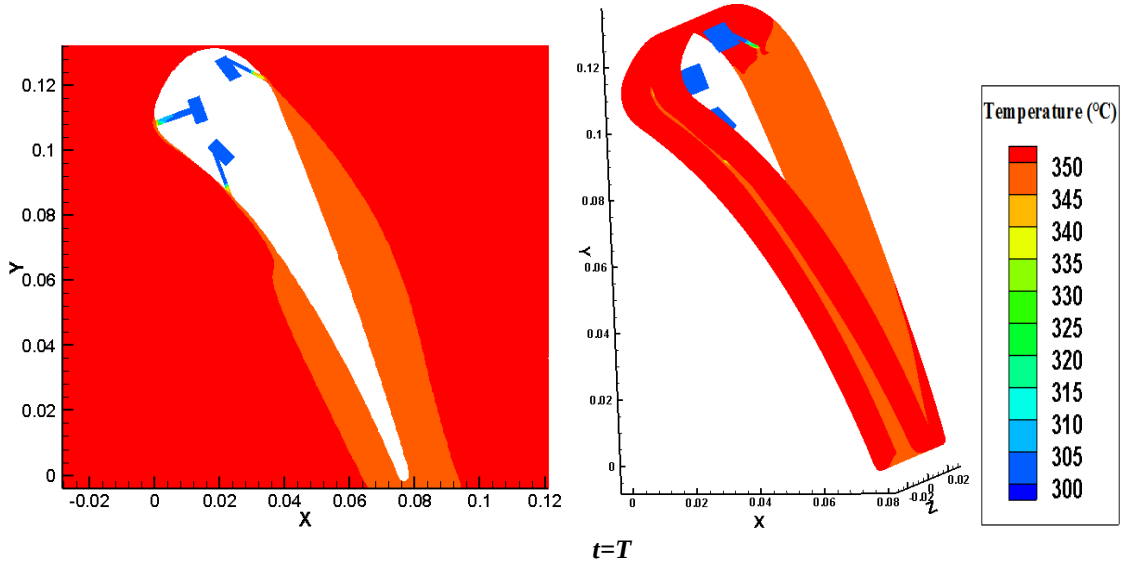

Fig. 10. Temperature distribution of different blade surfaces and its regions around at various time steps of a period with sinusoidal pulsed flow at frequency of 50 Hz and M=1

Figure 11 shows effectiveness distribution on blade surface at blowing ratio of 1. At this blowing ratio, effectiveness of various sections of blade at a cycle is changing. Effectiveness at downstream of injection hole is reduced due to separation of film cooling and the mixing of injection air with the mainstream in comparison with blowing ratio of 0.5.

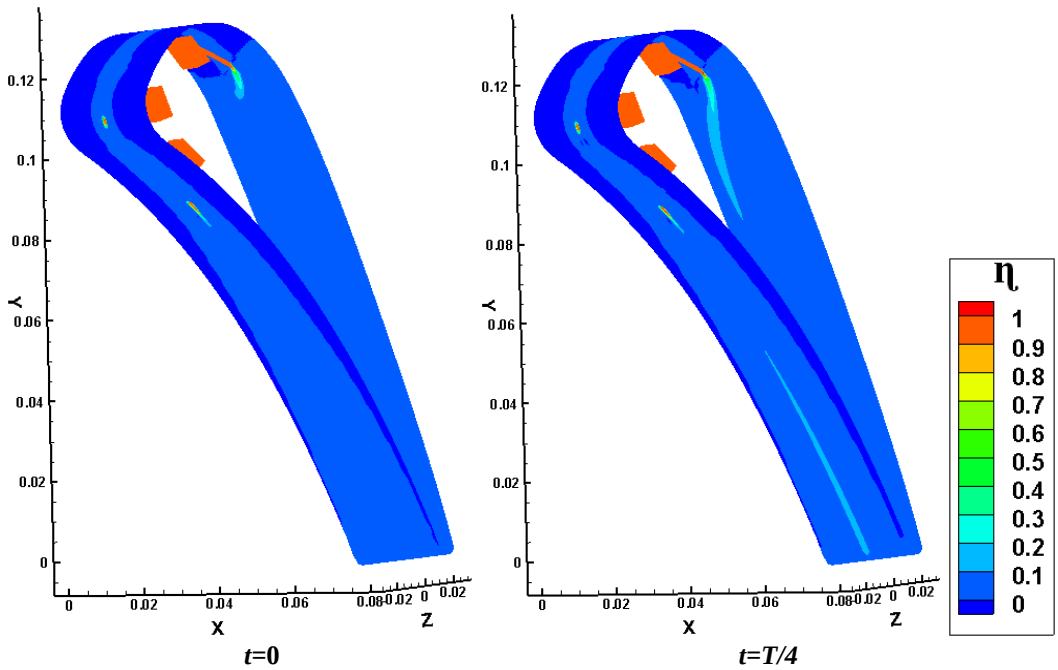

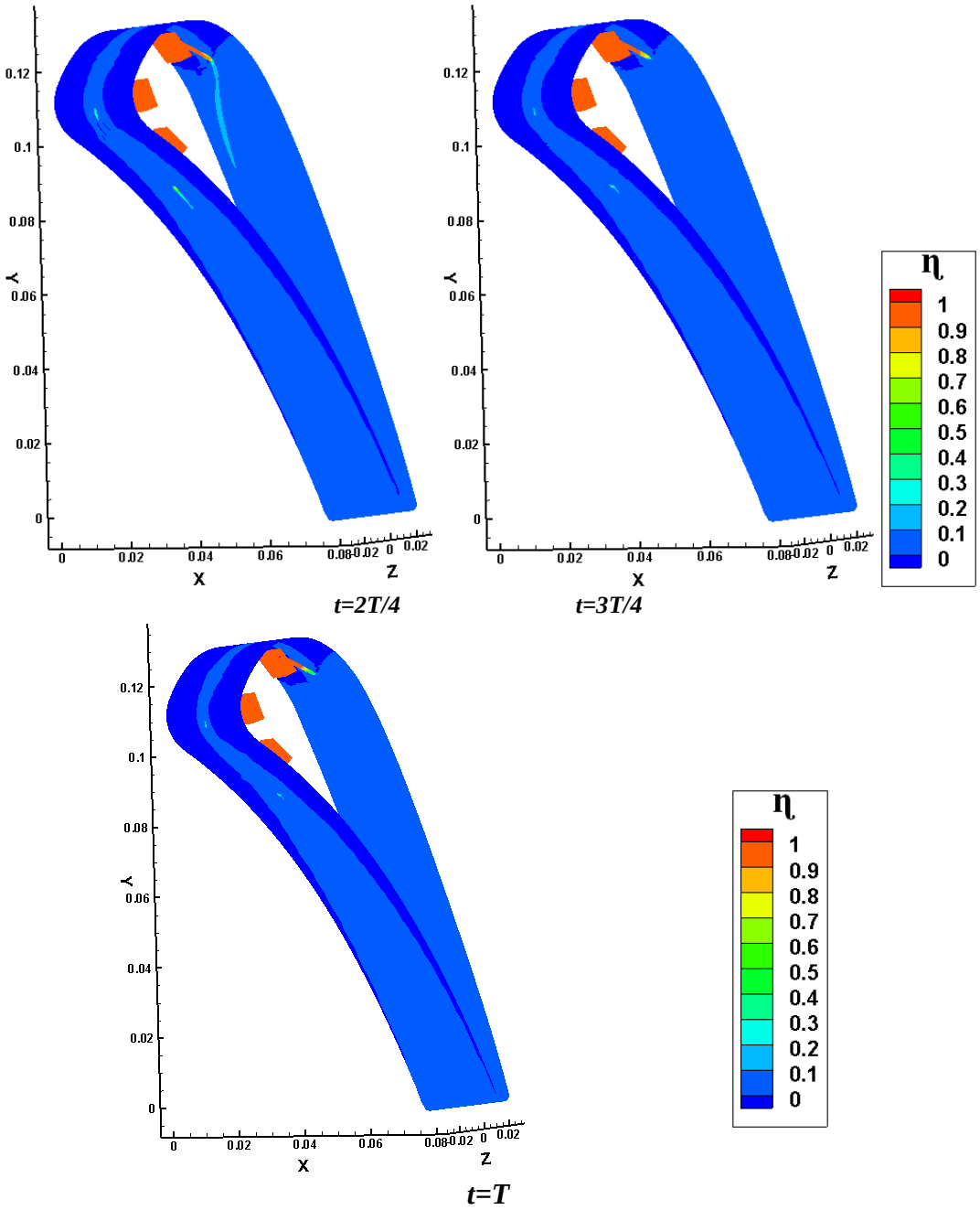

Fig. 11. Contours of blade film cooling effectiveness for various time steps of a cycle of sinusoidal pulsation at frequency of 50 Hz and M=1

For square wave flow, surface temperature contours of blade at various steps for a complete period time at blowing ratio of 2.5 is shown in Fig. 12. As it is evident from Fig. 12, at this blowing ratio, cooling air completely mixed with the mainstream and does not cover the surface at the leading edge, suction and pressure sides, also coolant air mixing with the mainstream causes decrease in mainstream temperature, and consequently reduces thermal efficiency of the turbine. Of course at this blowing ratio, downstream of suction and pressure surfaces of blade against the leading edge, possess a higher cooled air covering surface relative to lower blowing ratios. The reason for this phenomenon at suction and pressure surfaces is that the main flow velocity is greater than leading edge and local blowing ratio on suction and pressure side is less than leading edge. At low blowing

ratios, cooling air attaches to wall at suction and pressure surfaces, and with increasing the blowing ratio, more cooling air adhere to the blade surface, and as a result, cooled film covering and its effectiveness improves.

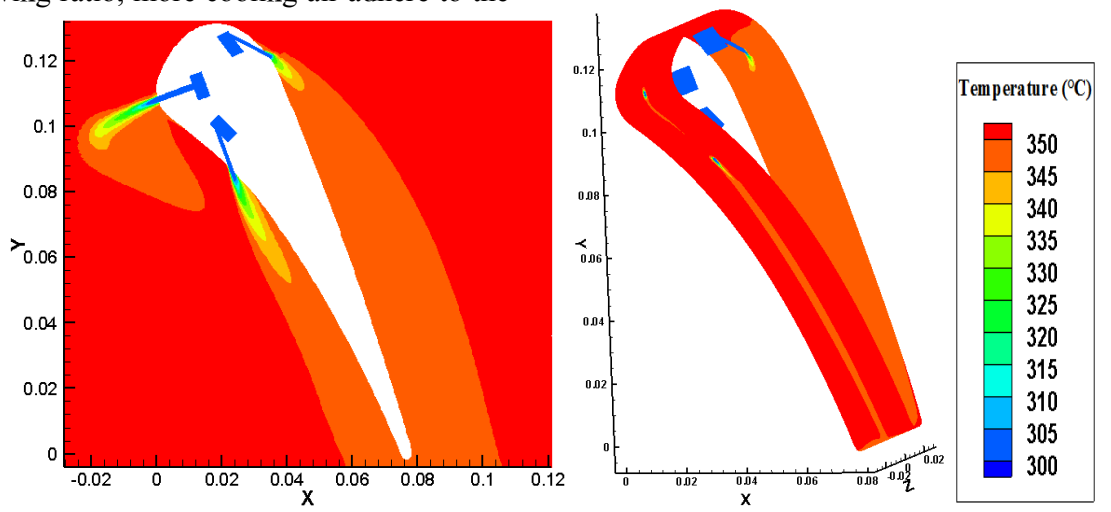

t=0

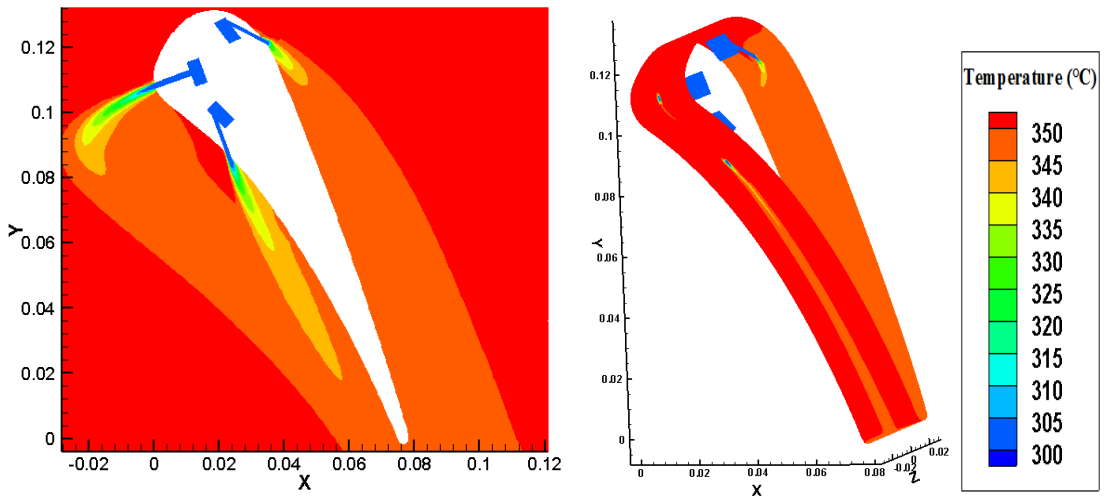

t=T/4

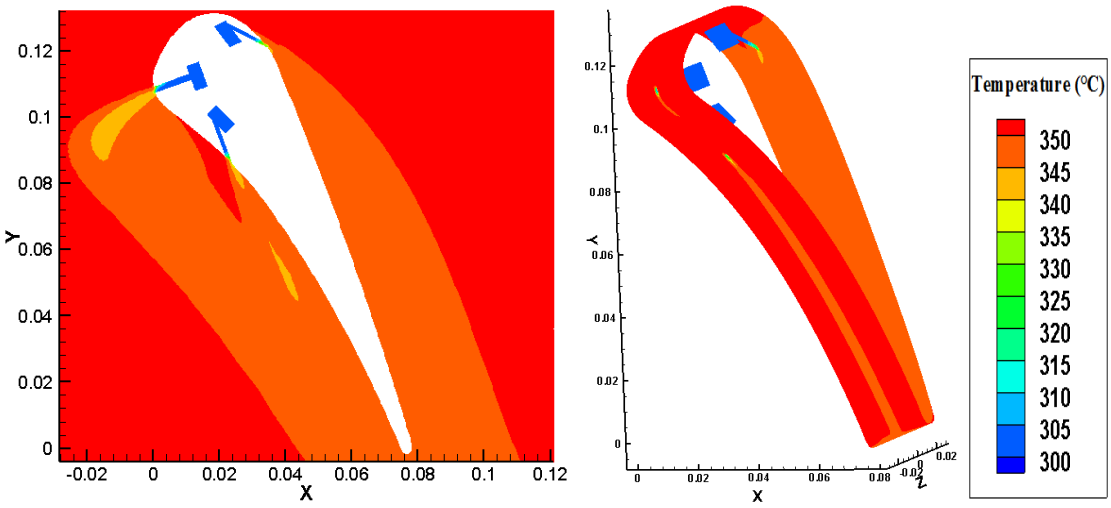

t=2T/4

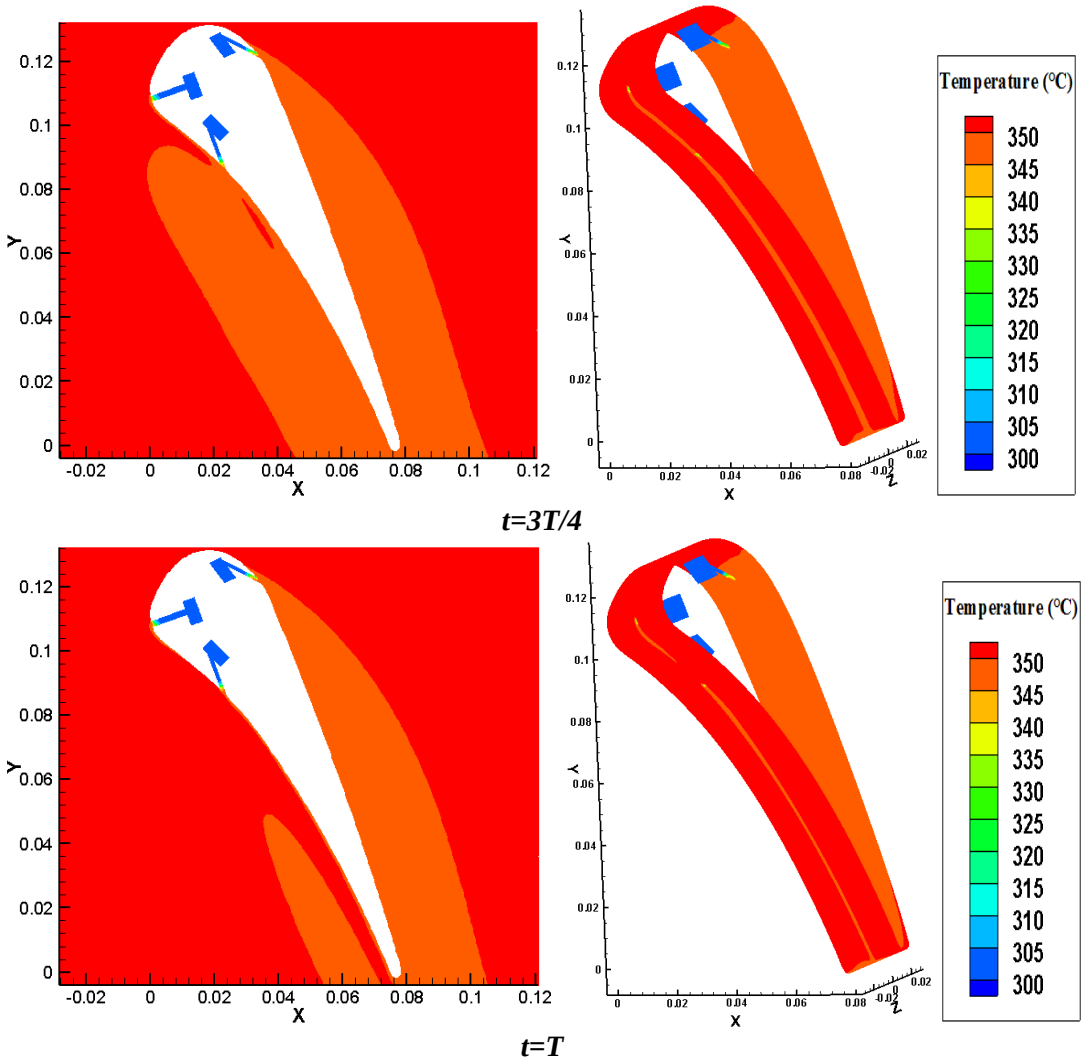

Fig. 12. Temperature distribution of different blade surfaces and its regions around at various time steps of a cycle with sinusoidal pulsed flow at frequency of 50 Hz and M=2.5

Figure 13 shows effectiveness distribution on blade surface at blowing ratio of 2.5. As is clear from, effectiveness distribution on leading edge is lower than other surfaces. Effectiveness values on pressure side and initial distances of downstream of suction side at blowing ratio of 2.5 are higher than other blowing ratios. For distances away downstream of suction side at blowing ratio of 2.5, film covering and its efficiency is lower than other blowing ratios. For large blowing ratios, due to better coverage of cooling air, effectiveness at initial distances of downstream of injection hole increases, but at distances away downstream, due to change at surface curvature, the possibility of separating the coolant from surface increases and therefore at farther downstream of injection hole at suction side, distribution of effectiveness is lower at blowing ratio of 2.5 compared with low blowing ratios.

Figure 14 compares temperature distribution and centerline effectiveness for a complete cycle of square wave cooling flow at different blowing ratios at downstream of blade leading edge. Averaged centerline film cooling effectiveness at downstream surface of injection hole for leading edge at blowing ratio of 0.5 has maximum value and at blowing ratio of 2.5 is the lowest. Averaged difference of effectiveness at these two blowing ratios is 47.7%.

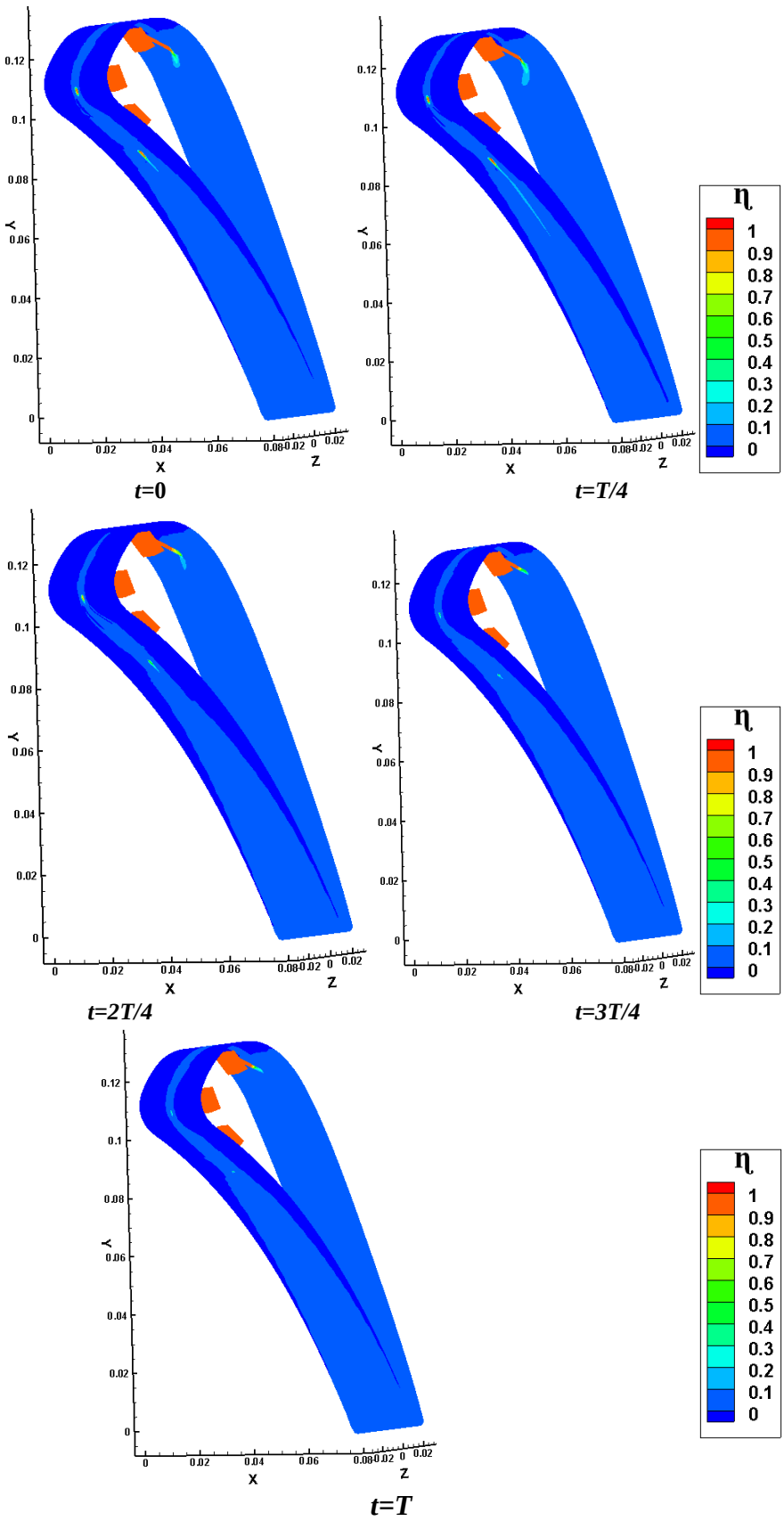

Fig. 13. Contours of blade film cooling effectiveness at various time steps of a period of sinusoidal pulsation at frequency of 50 Hz and M=2.5

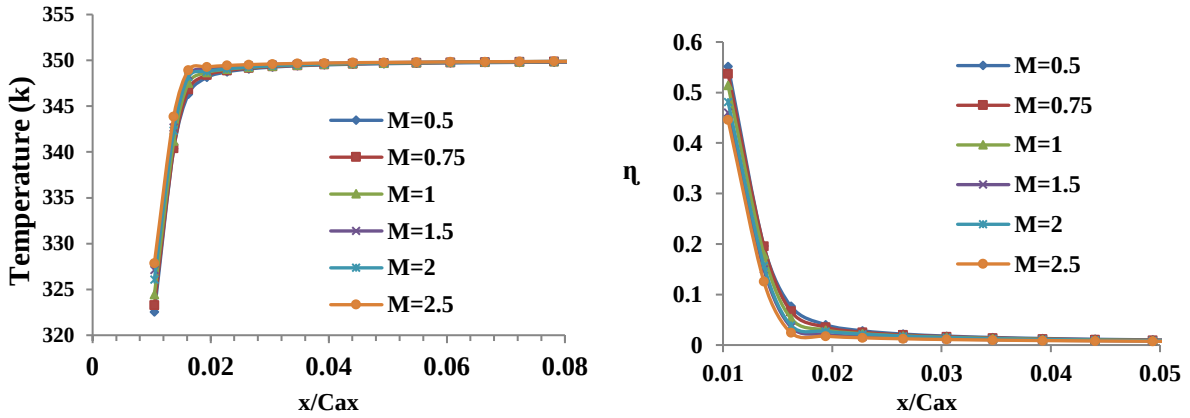

Fig. 14. Distribution of temperature and film cooling effectiveness at leading edge of the blade at various blowing ratios for sinusoidal pulsed flow at frequency of 50 Hz.

Figure 15 shows comparison of temperature distribution and centerline effectiveness for square pulsed flow at different blowing ratios at downstream of the pressure side of blade. As it can be seen, surface adiabatic temperature increases with increasing the blowing ratio and subsequently decreases film cooling effectiveness.

In this case, maximum averaged centerline effectiveness value obtained at blowing ratio of 0.5 and its lowest value is at blowing ratio of 1.5. Difference between the lowest and largest averaged effectiveness values on pressure side is 106.4%.

Figure 16 shows comparison of temperature distribution and centerline effectiveness for a cycle of cooling square pulse at various blowing ratios at downstream of blade suction surface. For suction side, surface temperature and, consequently, film cooling effectiveness distribution of square pulsation is less than pressure side at different blowing ratios. The averaged centerline film cooling effectiveness at blowing ratio of 2.5 is the largest value and at blowing ratio of 0.5 has the lowest value with a maximum difference of 9.06%.

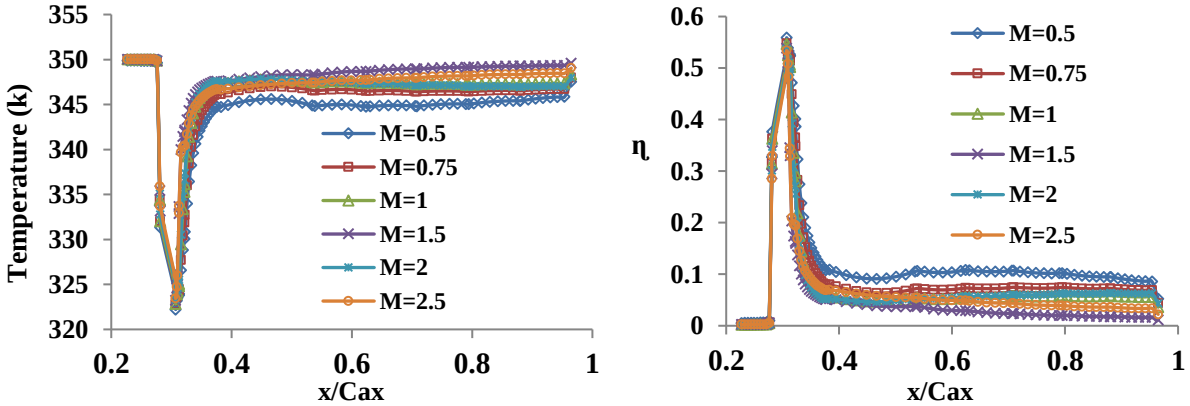

Fig. 15. Temperature and film cooling effectiveness distribution at downstream on the pressure side at different blowing ratios for sinusoidal pulsed flow at frequency of 50 Hz.

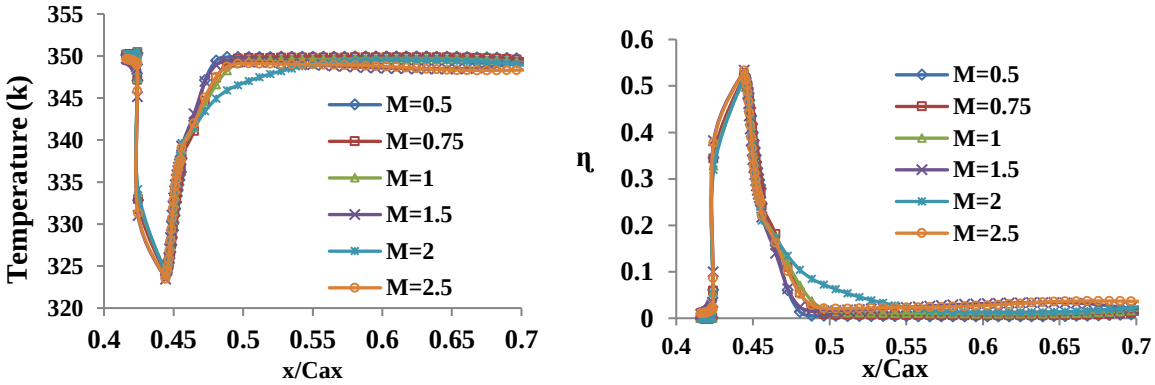

Fig. 16. Temperature and film cooling effectiveness distribution on downstream of the suction surface at different blowing ratios for sinusoidal pulsed flow at frequency of 50 Hz.

In this section, effect of mainstream Reynolds number on centerline film cooling effectiveness for square pulsed flow is investigated. Three Reynolds numbers of 37326, 74652 and 111978 were studied. Figure 17 shows effectiveness distribution on leading edge, pressure side and suction surface of blade for different Reynolds numbers at blowing ratio of 1. As it is seen, for pressure side, change of mainstream Reynolds number has the greatest effect on effectiveness distribution. At leading edge and suction side, averaged centerline effectiveness at Reynolds number of 74652 has its maximum value, but at pressure side at Reynolds number of 111978, the highest averaged centerline effectiveness value was obtained.

As the frequency of the square wave pulsating flow increases, the flow on-off time at a cycle decreases. The lift-off of the local jet increases under pulsation. Generally, increasing the frequency reinforces the overall film cooling effectiveness because with enhancing the frequency, pulsed flow approaches to the steady state flow.

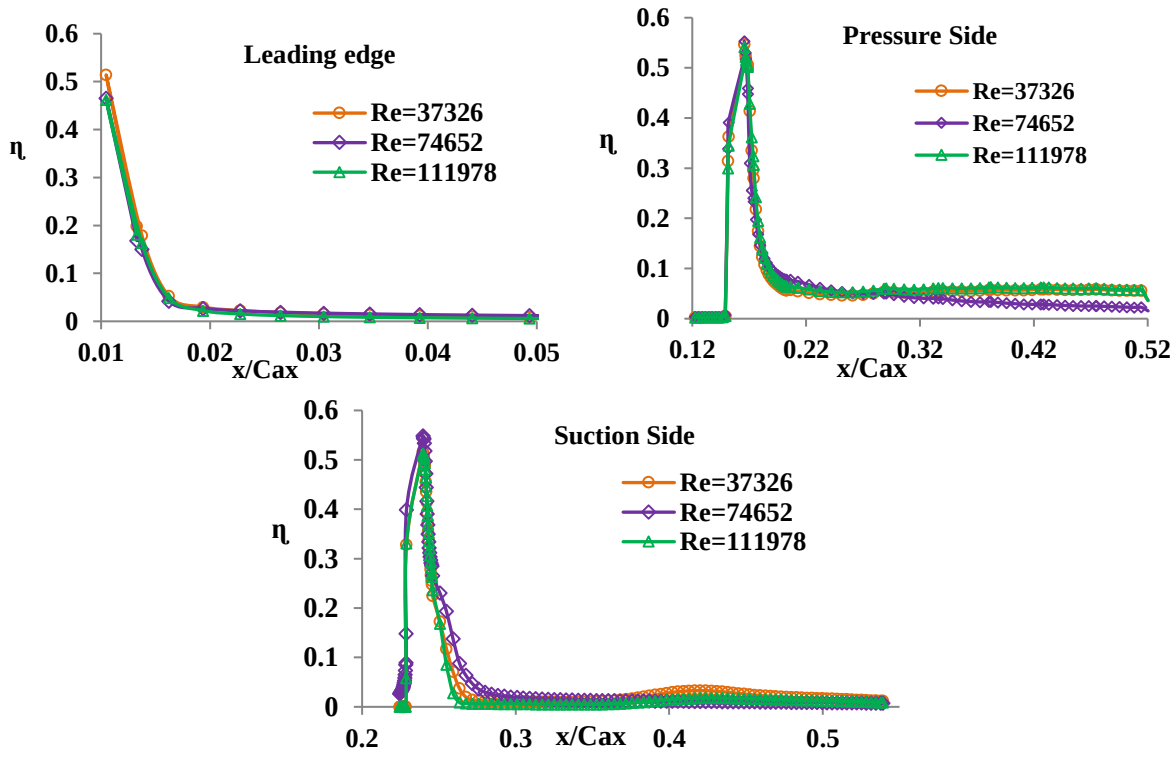

Fig. 17. Influence of Reynolds number on the film cooling effectiveness on leading edge, suction and pressure surfaces

4. Conclusions

In this research, effect of pulsed cooling air injection with square wave on film cooling performance of different surfaces of a turbine blade was numerically investigated. Finite volume method was used to solve flow governing equations and SST k-ω model was used to consider the effects of turbulence.
The obtained results showed that for steady state flow at blowing ratio of 0.5, surface temperature of downstream of injection hole at leading edge and pressure side was lower than other blowing ratios, resulting in averaged film cooling effectiveness at blowing ratio of 0.5 is more than other blowing ratios. For suction surface, average values of film efficiency at blowing ratio of 1.5 is maximum. For large blowing ratios, averaged pulsed film cooling effectiveness at leading edge and pressure surface is reduced compared to low and medium blowing ratios. This trend is reversed in the suction side. Changing coolant air mass flow rate at a square wave cycle causes change the size and strength of counter-rotating vortex pair, resulting in change the surface temperature distribution and, consequently, in contours of film cooling effectiveness at any time steps. Centerline averaged pulsating film cooling effectiveness distribution at downstream of injection hole on leading edge and pressure side of at blowing ratio of 0.5 and for suction side at blowing ratio of 2.5 had maximum values. Change of mainstream Reynolds number at pressure side had the greatest effect on the film cooling effectiveness but at suction surface and leading edge sections, effectiveness had slightly changing with Reynolds number.

References

[1] Zirak S., Ebrahimi H., Maissamy A.R., The Required Power of the MGT-40 Gas Turbine,Starter, Energy Equipment and Systems (2015) 3: 137-142.
[2] Foroutan H., M Rajabi-Zargarabadi F., Film Cooling Effectiveness in Single Row of Holes: First Moment Closure Modeling, Energy Equipment and Systems, (2013) 1: 5-18.
[3] Mousavi S.M., Nejat A., Kowsary F., Optimization of Turbine Blade Cooling with the Aim of Overall Turbine Performance Enhancement, Energy Equipment and Systems, (2017) 5: 71-83.
[4] Park S.H., Kang Y.J., Seo H.J., Kwak J.S., Kang Y.S., Experimental Optimization of a Fan-Shaped Film Cooling Hole with 30 Degrees-Injection Angle and 6-Hole Length-to-Diameter Ratio, International Journal of Heat and Mass Transfer (2019) 144: 118652.
[5] Abdelmohimen M.A., Mohiuddin A., Experimental Investigation of Film Cooling from Compound Angle Holes Supplemented by Secondary Holes, International Journal of Heat and Mass Transfer (2019) 144: 118678.
[6] Chen Z., Zhang Z., Li Y., Su X., Yuan X., Vortex Dynamics Based Analysis of Internal Crossflow Effect on Film Cooling Performance, International Journal of Heat and Mass Transfer (2019)145: 118757.
[7] Qingzong X., Qiang D., Pei W., Junqiang Z., Computational Study of Film Cooling and Flowfields on a Stepped Vane Endwall with a Row of Cylindrical Hole and Interrupted Slot Injections, International Journal of Heat and Mass Transfer (2019) 134: 796-806.
[8] Mousavi S.M., Rahnama S.M., Shape Optimization of Impingement and Film Cooling Holes on a Flat Plate Using a Feed Forward ANN and GA, Energy Equipment and Systems (2018) 6: 247-259.
[9] Zhang C., Wang J., Luo X., Song L., Li J., Feng Z., Experimentally Measured Effects of Height and Location of the Vortex Generator on Flow and Heat Transfer Characteristics of theFlat-Plate Film Cooling, International Journal of Heat and Mass Transfer (2019) 141: 995-1008.
[10] Liu Y., Luo Y., Transient Simulation of Pulsed Purge Film Cooling on Flow and Thermal Characteristics of a Turbine Endwall, Applied Thermal Engineering (2019) 161: 114208.
[11] Hosseini Baghdad Abadi S.M., Zirak S., Rajabi Zargar Abadi M., Numerical

Simulation of the Sinusoidal Wave Pulsed Film Cooling Effectiveness Due to the Changing Cooling Injection Parameters, Journal of Modares Mechanical Engineering (2019) 19: 191-200.

[12] Womack K.M., Volino R.J., Schultz M.P., Combined Effects of Wakes and Jet Pulsing on Film Cooling, Journal of Turbomachinery, (2008) 130: 041010.

[13] Borup D.D., Fan D., Elkins C.J., Eaton J.K., Experimental Study of Periodic Free Stream Unsteadiness Effects on Discrete Hole Film Cooling in Two Geometries, Journal of Turbomachinery (2019) 141: 061006.

[14] Abdous R., Zirak S., Performance Evaluation of Trapezoidal Teeth Labyrinth Seal, Energy Equipment and Systems (2017) 5: 265-273.

[15] Hosseini Baghdad Abadi S.M., Zirak S., Rajabi Zargarabadi M., Numerical Investigation of the Effect of Sinusoidal Pulsating Cooling Air on Film Cooling Effectiveness of Leading Edge, Pressure and Suction Side of a Turbine Blade, Journal of Solid and Fluid Mechanics (2019) 9: 227-247.

[16] Montomoli F., D'Ammaro A., Uchida S., Numerical and Experimental Investigation of a New Film Cooling Geometry with High P/D Ratio, International Journal of Heat Mass Transfer (2013) 66: 366-375.

[17] Lin Y.L., Shih T.P., Film Cooling of a Cylindrical Leading Edge with Injection Through Rows of Compound-Angle Holes, Journal of Heat Transfer (2001) 123: 645-654.

[18] He W., Deng Q., Zhou W., Gao T., Feng Z., Film Cooling and Aerodynamic Performances of a Turbine Nozzle Guide Vane with Trenched Cooling Holes, Applied Thermal Engineering (2019) 150: 150-163.

[19] Ke Z., Wang J., Conjugate Heat Transfer Simulations of Pulsed Film Cooling on an Entire Turbine Vane, Applied Thermal Engineering (2016) 109: 600-609.

[20] Wang H., Tao Z., Zhou Z., Han F., Li H., Experimental and Numerical Study of the Film Cooling Performance of the Suction Side of a Turbine Blade Under the Rotating Condition, International Journal of Heat and Mass Transfer (2019) 136: 436-448.

[21] Menter F.R., Two-Equation Eddy-Viscosity Turbulence Models for Engineering Applications, AIAA Journal (2002) 40: 254-266.

[22] Mohajer A., Zirak S., Abbasi E., Development of a Compression System Dynamic Simulation Code for Testing and Designing of Anti-Surge Control System, Energy Equipment and Systems (2019) 7: 99-110.

[23] Hylton L.D., Mihelc M.S., Turner E.R., Nealy D.A., York R.E., Analytical and Experimental Evaluation of the Heat Transfer Distribution Over the Surfaces of Turbine Vanes, NACA, Report CR-168015.

[24] Zhaoqing K., Wang J., Numerical Investigations of Pulsed Film Cooling on an Entire Turbine Vane, Applied Thermal Engineering (2015) 87: 117-126.

[25] Charmchi M., Zirak S., Numerical Simulation of Incompressible Turbulent Flow in Shrouded Disk System with Radial Outflow, Energy Equipment and Systems (2019) 7: 1-10.

[26] Hosseini Baghdad Abadi S.M., Zirak S., Rajabi Zargar Abadi M., Experimental and Numerical Investigation of Square Wave Pulsed Film Cooling Performance on a Flat Plate, Journal of Modares Mechanical Engineering (2020) 20:329-340.

[27] Hosseini Baghdad Abadi S.M., Zirak S., Rajabi Zargar Abadi M., Numerical Investigation of the Effect of Coolant Injection Angle on the Pulsed Film Cooling Effectiveness of Square Wave Flow on Flat Plate, Amirkabir Journal of Mechanical Engineering (2020) 52:161-170.

[28] Hosseini Baghdad Abadi S.M., Zirak S., Rajabi Zargar Abadi M., Numerical Study of the Effect of Rotation on the Film Cooling Effectiveness of a Turbine Blade with Square Pulsating Cooling Flow, Journal Fluid Mechanics and Aerodynamics (2019) 8: 113-130.

[29] Hosseini Baghdad Abadi S.M., Zirak S., Rajabi Zargar Abadi M., Effect of pulsating injection and mainstream attack angle on film cooling performance of a gas turbine blade, Physics of Fluids (2020) 32: 117102.